# Selective Reduction Mechanism of Graphene Oxide Driven by the Photon Mode *versus* the Thermal Mode

## *Supporting information*

Masaki Hada*, Kiyoshi Miyata, Satoshi Ohmura, Yusuke Arashida, Kohei Ichiyanagi, Ikufumi Katayama, Takayuki Suzuki, Wang Chen, Shota Mizote, Takayoshi Sawa, Takayoshi Yokoya, Toshio Seki, Jiro Matsuo, Tomoharu Tokunaga, Chihiro Itoh, Kenji Tsuruta, Ryo Fukaya, Shunsuke Nozawa, Shin-ichi Adachi, Jun Takeda, Ken Onda*, Shin-ya Koshihara, Yasuhiko Hayashi, and Yuta Nishina*

*Emails: hada.masaki.fm@u.tsukuba.ac.jp (Masaki Hada),
konda@chem.kyushu-univ.jp (Ken Onda),
nisina-y@cc.okayama-u.ac.jp (Yuta Nishina)

### Table of Contents

## 1. Static characterization of graphene oxide

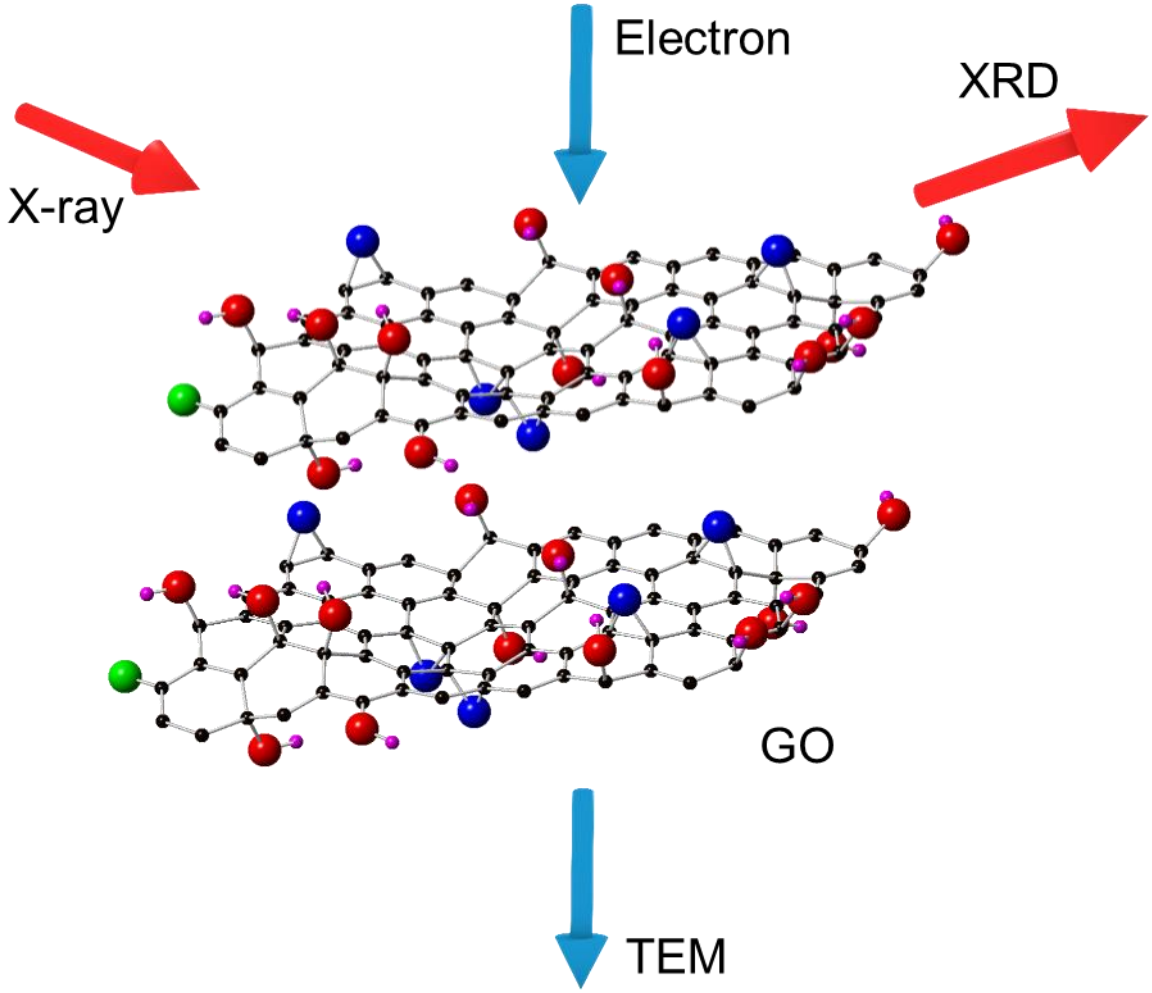


Figure S1. Schematic showing of GO and the geometry of GO used for static measurements (XRD) and electron diffraction using TEM. For the XRD measurements in reflection mode, GO is coated on glass substrates. For the electron diffraction measurements in transmission mode, GO is coated on SiN membrane substrates. The black, pink, red, blue, green balls represent carbon atoms, hydrogen atoms, and oxygen atoms in hydroxyl groups, oxygen atoms in epoxy groups, and oxygen atoms in carbonyl groups, respectively. The sheet of GO is a stacked single layer, indicating that the GO layers do not have lattice correlations to each other.

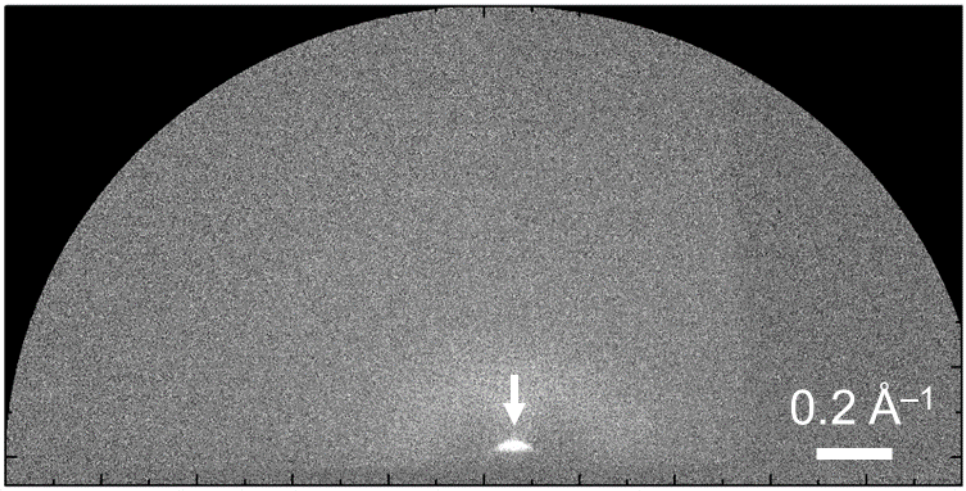


Figure S2. Reflection-mode synchrotron XRD[S1,S2] image of GO, with the white arrow showing the diffraction spot corresponding to the (0001) plane of GO. From the reflection mode, only the diffraction from the (0001) plane was obtained from GO, suggesting that the planes of GO are parallel to the substrate and are stacked on top of each other.

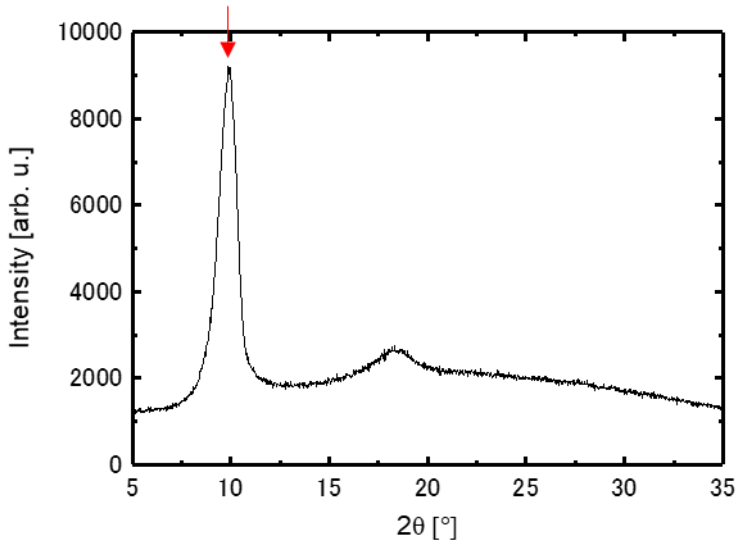


Figure S3. Powder XRD profile of GO. The peak indicated by the red arrow is ascribed to the $(0001)$ plane of GO ($2\theta \sim 10°$). According to the XRD profiles of GO, the lattice distance of the $(0001)$ plane is calculated to be ~9 Å using the Bragg's equation ($2\sin\theta = n\lambda$). The broad peak at $2\theta \sim 17°$ is attributed to the glass substrate.

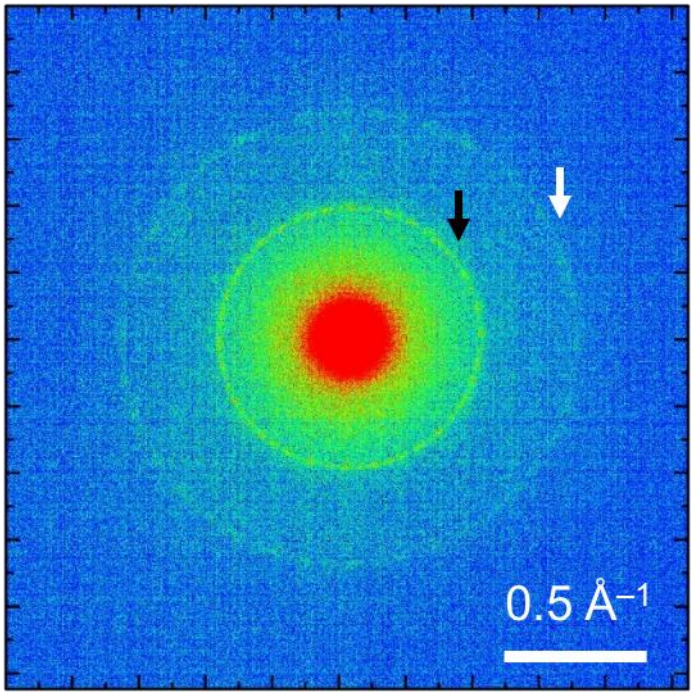


Figure S4. Electron diffraction image acquired using TEM in transmission mode, in which the black and white arrows indicate the diffraction rings corresponding to the $(10\bar{1}0)$ and $(11\bar{2}0)$ planes of GO, respectively. The electron acceleration energy was set to 80 keV to suppress electron impact-induced damage to GO.[S3]

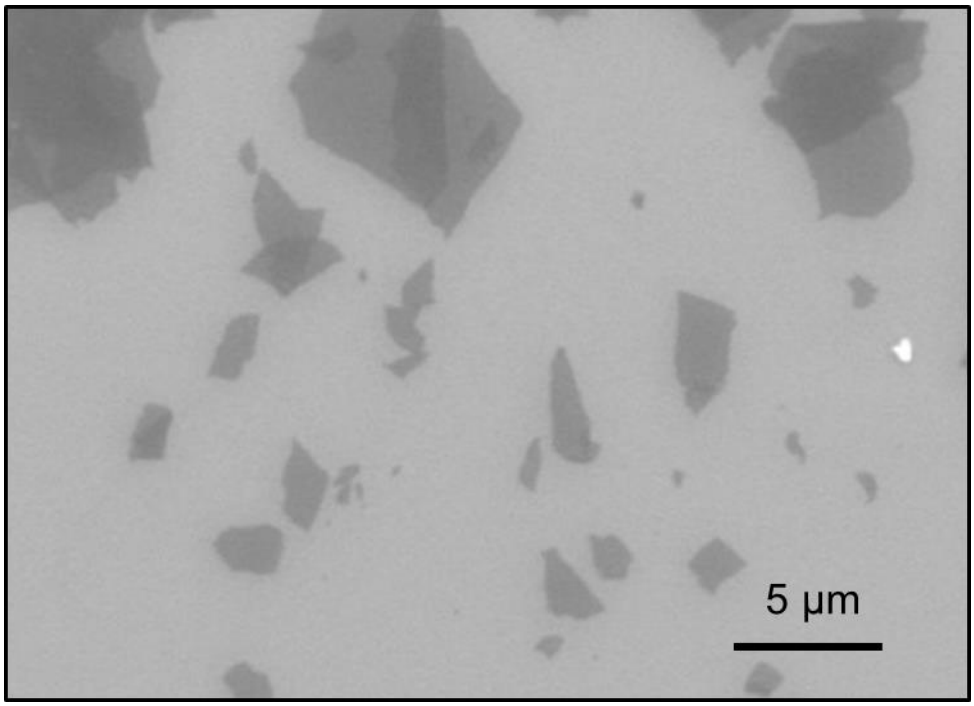


Figure S5. SEM image of GO. The image corresponds to the results obtained from XRD measurements, and thus the planes of GO are parallel to the substrate and stacked on top of each other.

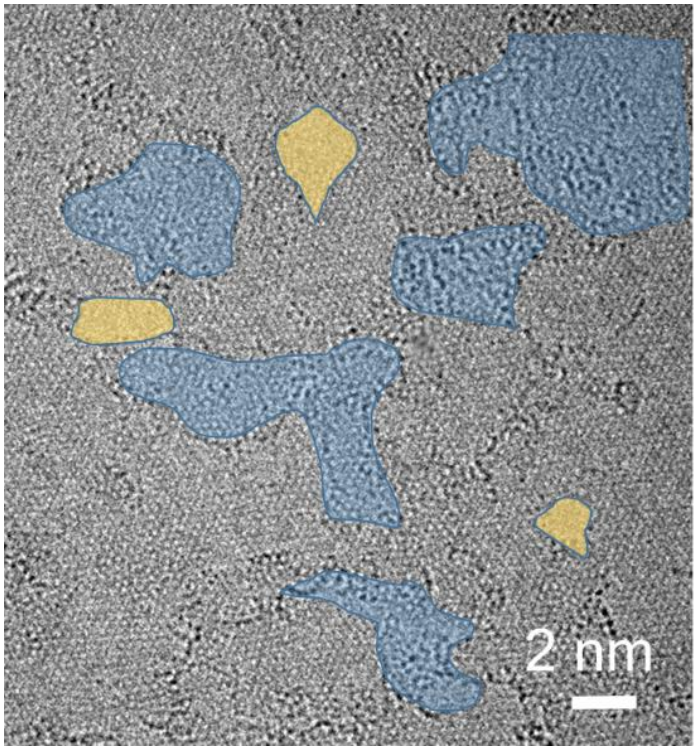


Figure S6. High-resolution TEM image of a single layer of GO. The electron acceleration energy was set to 80 keV to suppress electron impact-induced damage to GO.[S3] The observed images resembled images of rGO previously reported by Gómez-Navarro *et al.*[S3] GO should have three main distinct areas, *i.e.*, a fully oxidized area (blue), an area that retains a graphitic structure (gray), and holes (yellow).

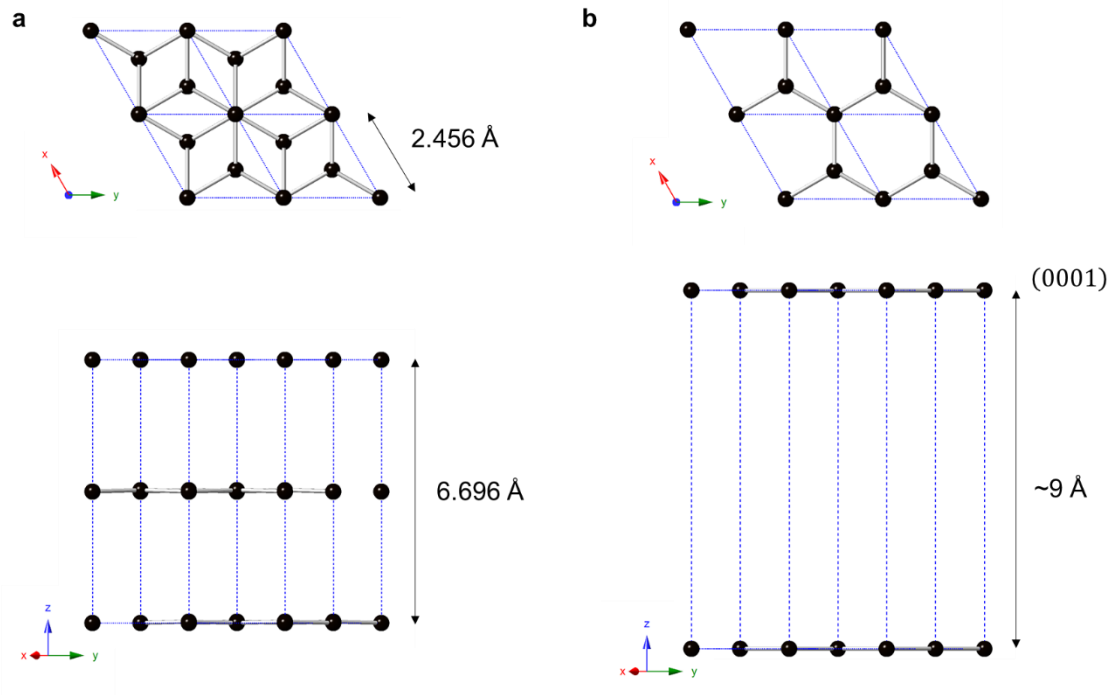


Figure S7. Lattice model of GO. Graphene and GO are two-dimensional materials, and three-dimensional model lattices for graphene and GO have not been reported. We modified the hexagonal lattice of graphite (a) to create the lattice model of GO. The hexagonal lattice of graphite resides in space group of $P6_3mc$, and the lengths of *a*- and *c*-axes are 2.456 and 6.696 Å, respectively.[S4] The GO layers do not have lattice correlations with each other, and the distance of the $(0001)$ plane is ~9 Å. Thus, the model of the GO structure is presented in (b), where the oxygen functional groups are simplified.

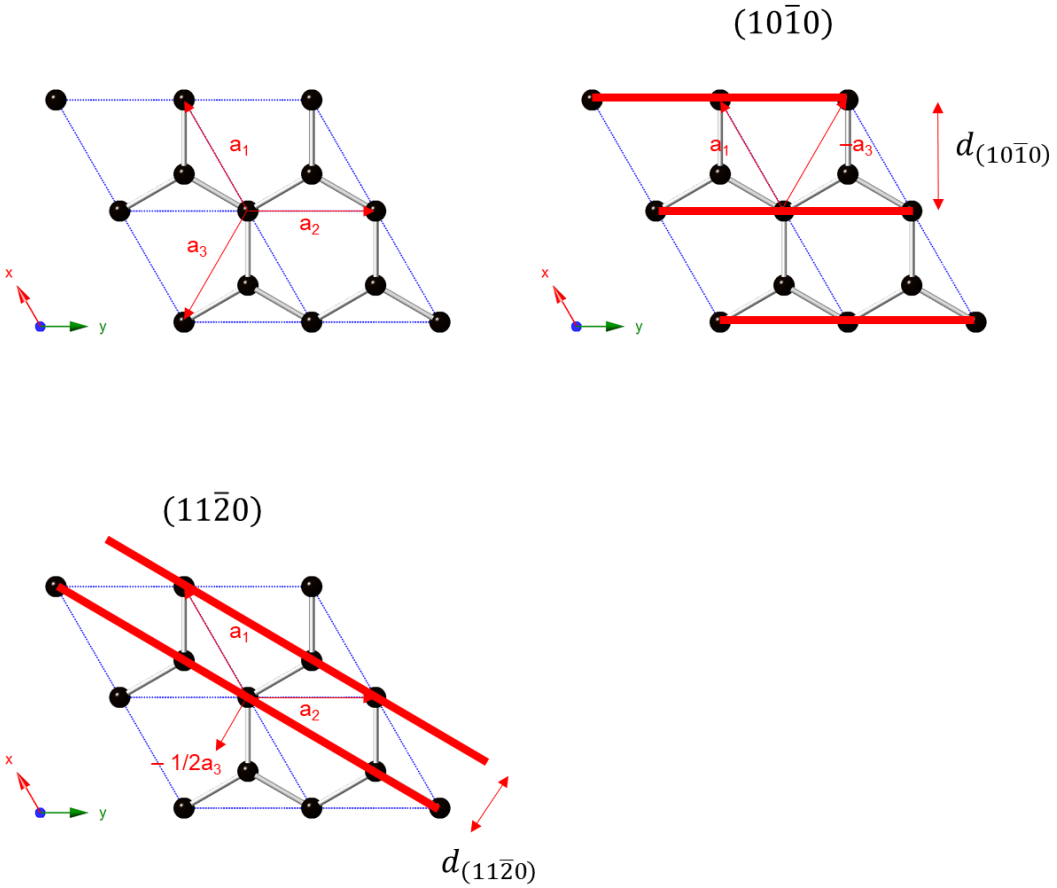


Figure S8. Distances of the $(10\bar{1}0)$ and $(11\bar{2}0)$ planes of GO. The lateral plane distances were determined from the lattice model of GO shown in Figure S7. According to the geometry, the average C–C bond length ($d_{\text{C-C}}$) is calculated from the distances of the $(10\bar{1}0)$ ($d_{(10\bar{1}0)}$) and $(11\bar{2}0)$ ($d_{(11\bar{2}0)}$) planes using the following equation:

$$d_{\text{C-C}} = \frac{2}{3} d_{(10\bar{1}0)} = \frac{2}{\sqrt{3}} d_{(11\bar{2}0)}.$$

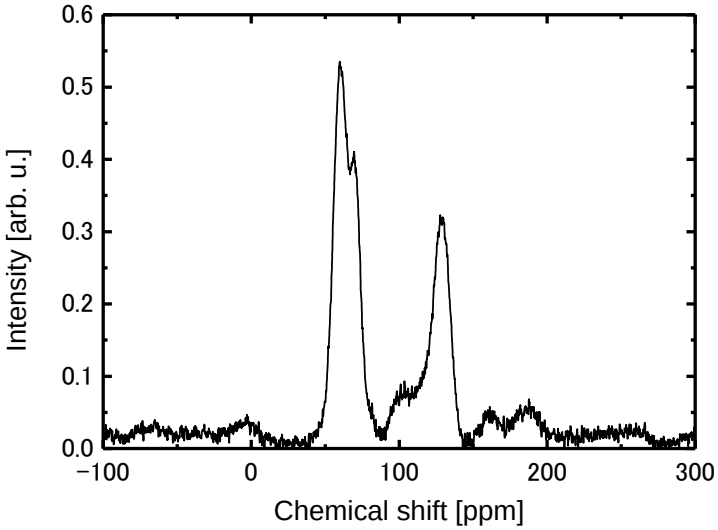


Figure S9. Solid-state $^{13}C$ NMR spectrum of GO. The peaks at the chemical shifts of 60, 70, and 130 ppm correspond to C–O–C, C–OH, and the $sp^2$ carbon, respectively.[S5]

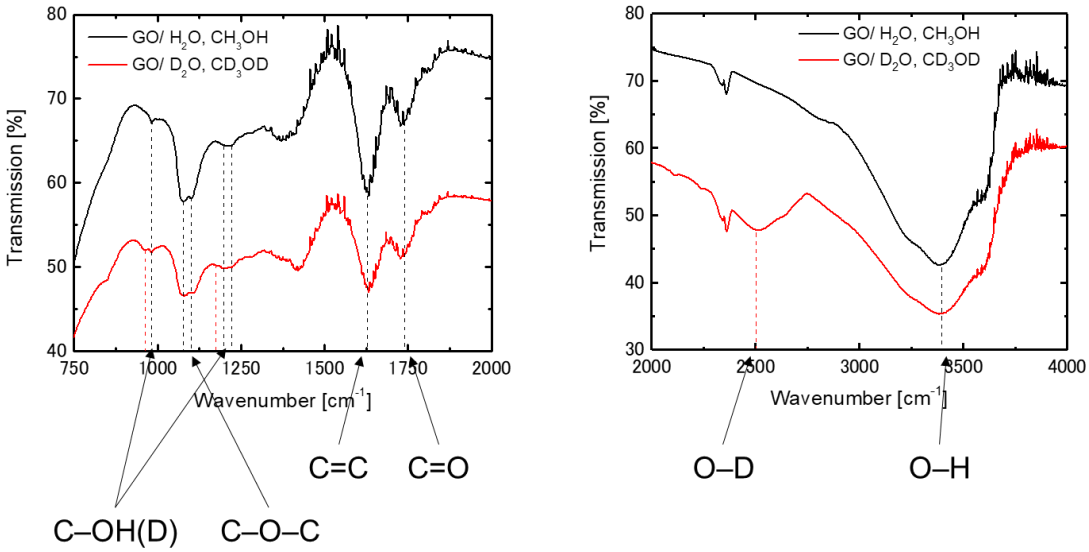


Figure S10. Fourier transform infrared spectrum of GO. Each peak is assigned to a corresponding bond, as indicated.[S6] The vibrational modes in the fingerprint region (wavenumbers of 800–1300 $cm^{-1}$) are related to C–C or C–O bonds. We compared the spectra of GO dispersed in $H_2O$/ $CH_3OH$ solution and $D_2O$/$CD_3OD$ solution to classify the peaks in the finger-print region. During the drying process, some of the D atoms in GO dispersed in the $D_2O$/$CD_3OD$ solution were also replaced by H atoms. The vibrational peak assignment is summarized in Table S1.

Table S1. Vibrational peak assignment in IR spectra

| No. | $k_{obs}$ [$cm^{-1}$] | Functional group |
|---|---|---|
| 1 | 982 | GO–OH, hydroxyl group on GO |
| 2 | 1075 | GO–O, epoxy group on GO |
| 3 | 1100 | GO–O, epoxy group on GO |
| 4 | 1200 | GO–OH, hydroxyl group on GO |
| 5 | 1220 | GO–OH, hydroxyl group on GO |
| 6 | 1630 | C=C in GO |
| 7 | 1735 | C=O, carbonyl group on GO |
| 8 | 3400 | O–H in GO |

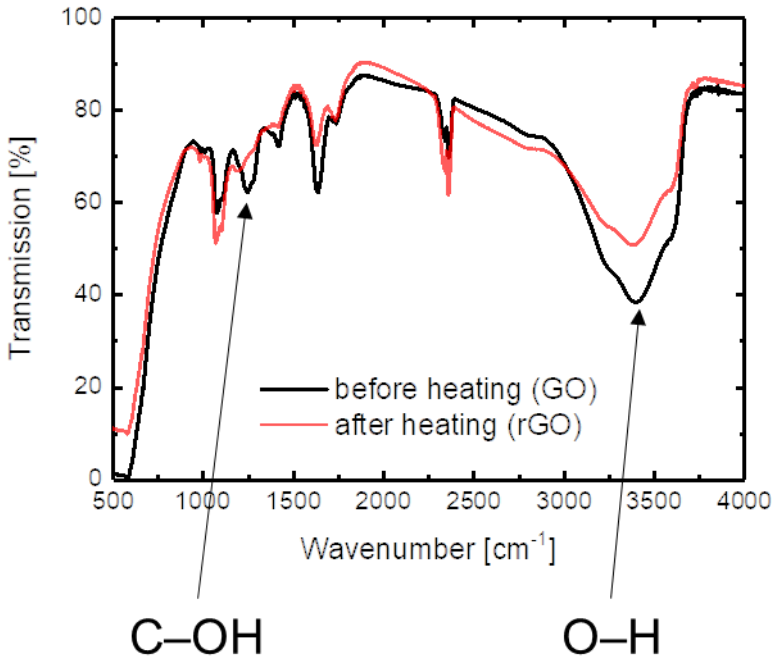


Figure S11. Fourier transform infrared spectra of GO before and after heating (423 K). After heating, the vibrational peak related to the O–H bonds (3400 $cm^{-1}$) decreases, and the peaks related to the GO–OH bonds (1200 and 1220 $cm^{-1}$) decrease and shift.

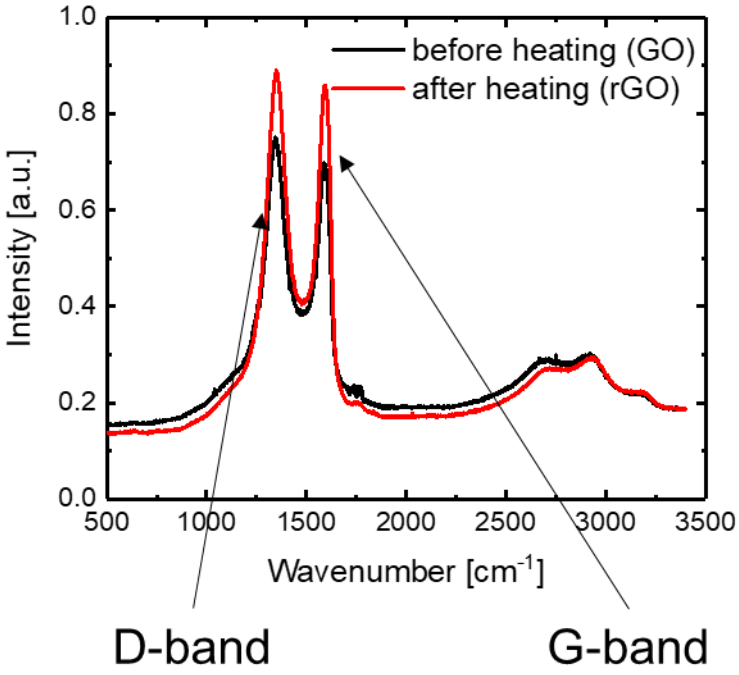


Figure S12. Raman spectra of GO before and after heating (423 K). The peaks corresponding to the D-band (1360 $cm^{-1}$) and G-band (1590 $cm^{-1}$) in GO are observed before and after heating.

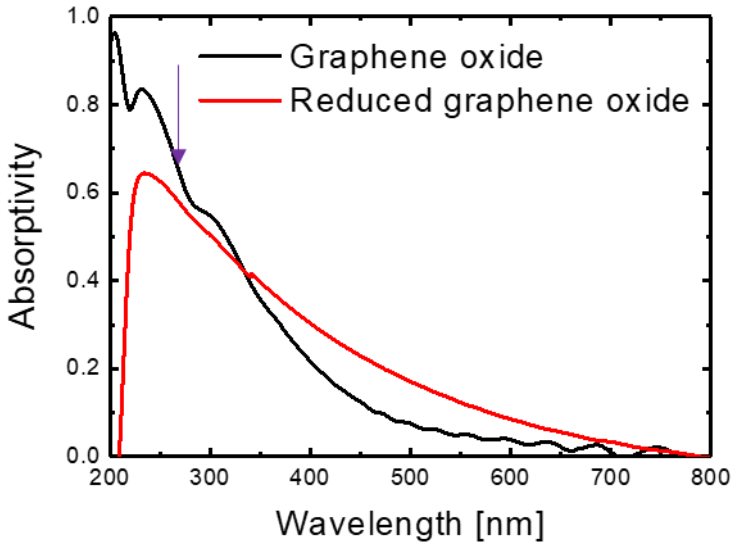


Figure S13. UV-visible spectrum (V-670, Jasco) of GO and thermally reduced GO featuring a strong π→π* band in the UV range. The thickness (*d*) of the films was 350 nm. The employed photoexcitation wavelength (266 nm) is indicated by the purple arrow (~65%). According to the following equation, the linear absorption coefficient (*l*) at a wavelength of 266 nm is 330 nm:

$$T = 1 - A = \exp(-\frac{d}{l})$$

where $T$ and $A$ are the transmission and absorptivity, respectively. For ultrafast time-resolved electron diffraction, the sample thickness was 70 nm, and the absorptivity of the light at a wavelength of 266 nm was 19%. For the pump light at a fluence of 2 mJ/cm$^2$, we increased the temperature of GO by 54 K, and we used a density of 1.1 g/cm$^3$ and a specific heat of 1 J/g·K. For the time-resolved IR vibrational spectroscopy, the sample thickness was 0.7 μm and the absorptivity of the light at a wavelength of 266 nm was 88%.

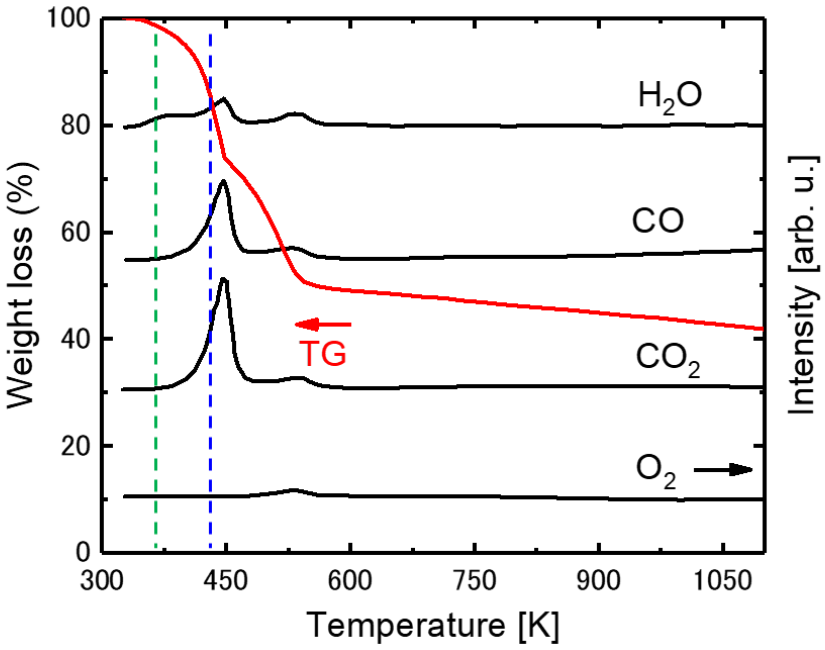


Figure S14. Results of thermogravimetric (TG) and mass-spectrometry (MS) analyses of GO at increasing temperatures. The loss of adsorbed water molecules at ~370 K is indicated by a green dashed line, whereas the loss of water, carbon monoxide, and carbon dioxide at ~420 K is indicated by a blue dashed line. TG-MS spectra were recorded with a RIGAKU Thermo plus EVO2 analyzer coupled to a Shimadzu GC-MS QP2010 instrument using He (99.999%) as a carrier gas (300 mL/min) and a heating rate of 6°C/min. The MS measurement was performed in the SIM mode to detect target molecules.

## 2. DFT and MM2 calculations for graphene oxide

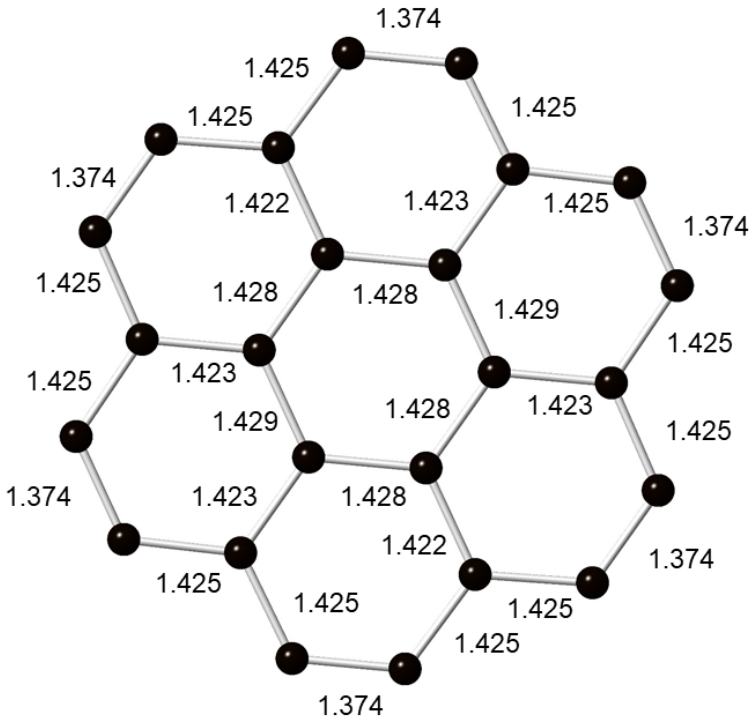


Figure S15. Model of the graphene structure base on DFT calculations featuring bond lengths (in Å) obtained from B3LYP/6-31G** level calculations. The average bond length was determined to be 1.415 Å, and black spheres indicate carbon atoms.

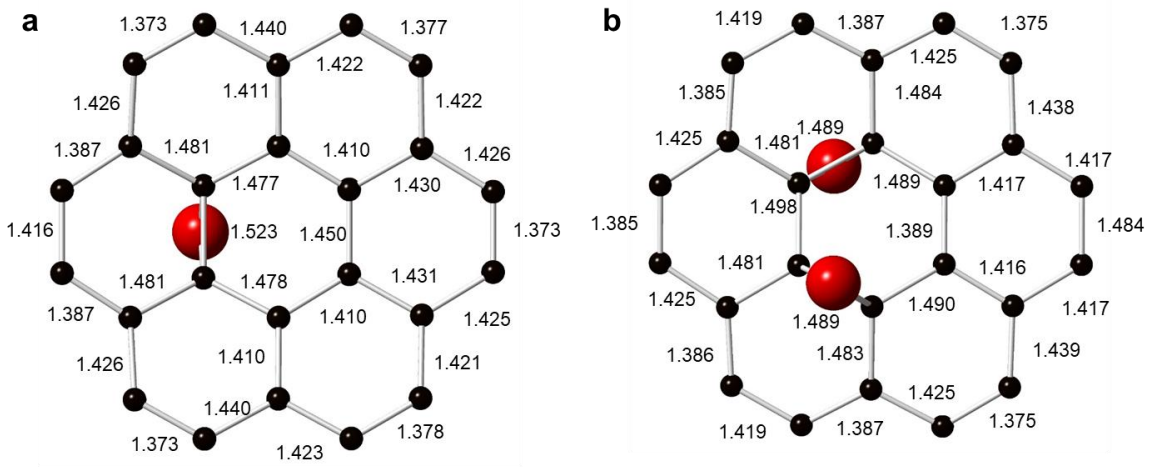


Figure S16. Models of GO structures obtained using DFT calculations featuring one (a) or two (b) oxygen atoms present in epoxy functional groups, and the bond lengths (in Å) obtained from B3LYP/6-31G** level calculations are shown. The average bond lengths of S2a and S2b were determined to be 1.424 and 1.434 Å, respectively. Red spheres indicate oxygen atoms.

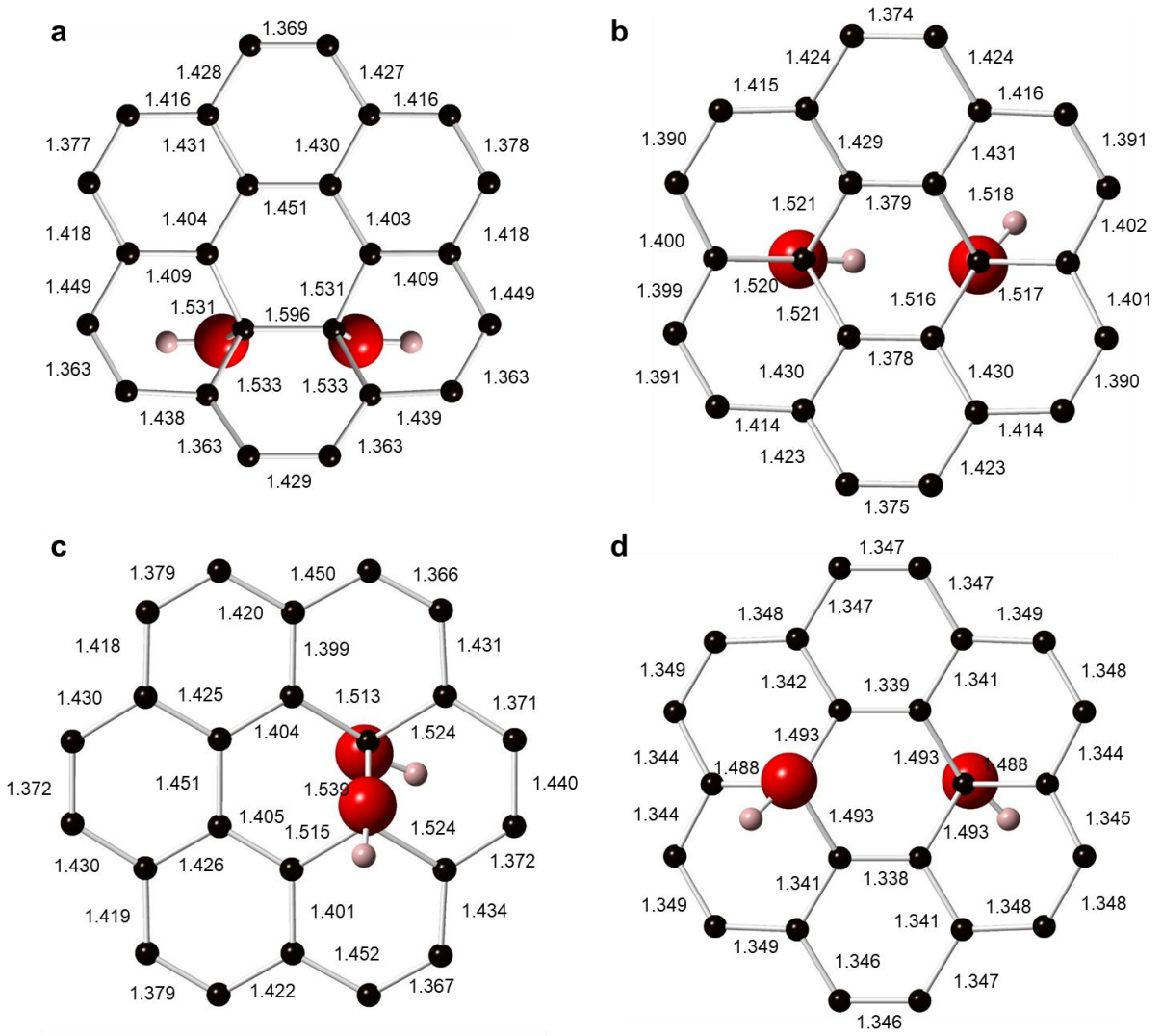


Figure S17. Models of GO structures obtained using DFT calculations featuring oxygen atoms present in hydroxyl groups, and the bond lengths (in Å) obtained from B3LYP/6-31G** level calculations are shown. The average bond length was determined to be 1.417 Å. Pink spheres indicate hydrogen atoms.

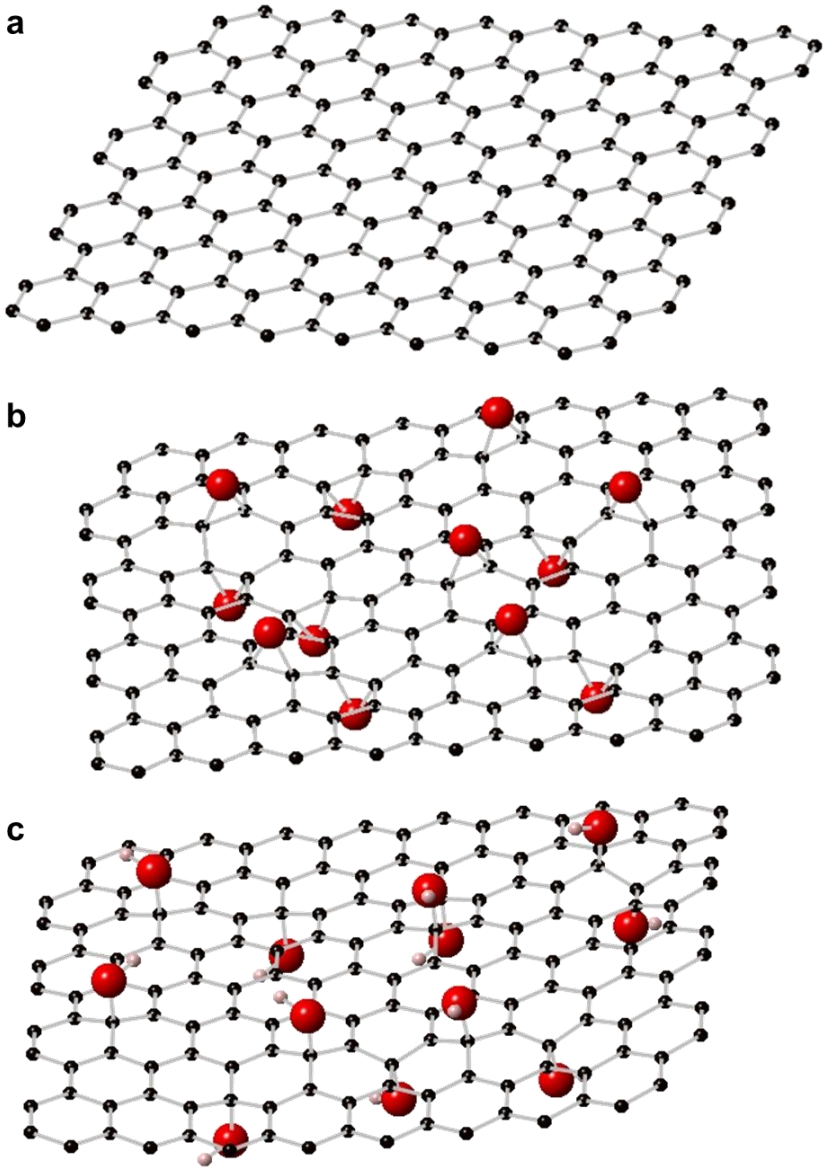


Figure S18. Models of the structure of (a) graphene, (b) GO with oxygen atoms present in epoxy groups, and (c) GO with oxygen atoms present in hydroxyl groups used for MM2 calculations.

## 3. Transient absorption of graphene oxide

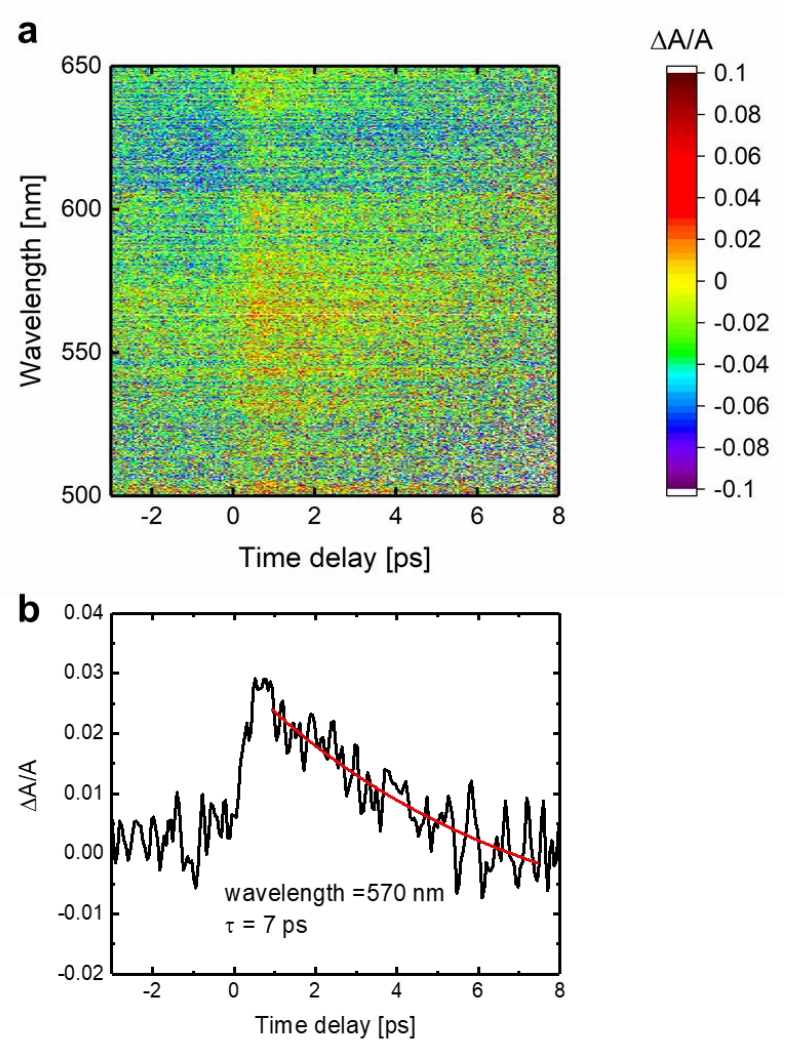


Figure S19. Single shot transient absorption spectra. (a) Two-dimensional map of the single shot transient absorption as functions of the time delay and wavelength. The details of the experiment are provided elsewhere.[S7] The incident fluence of the UV pulse (wavelength of 266 nm and pulse duration of 120 fs) was set to 1.5 mJ/cm$^2$. (b) Transient absorption spectrum at a wavelength of 570 nm. The red line is the fit obtained using an exponential decay curve with a decay time of 7 ps.

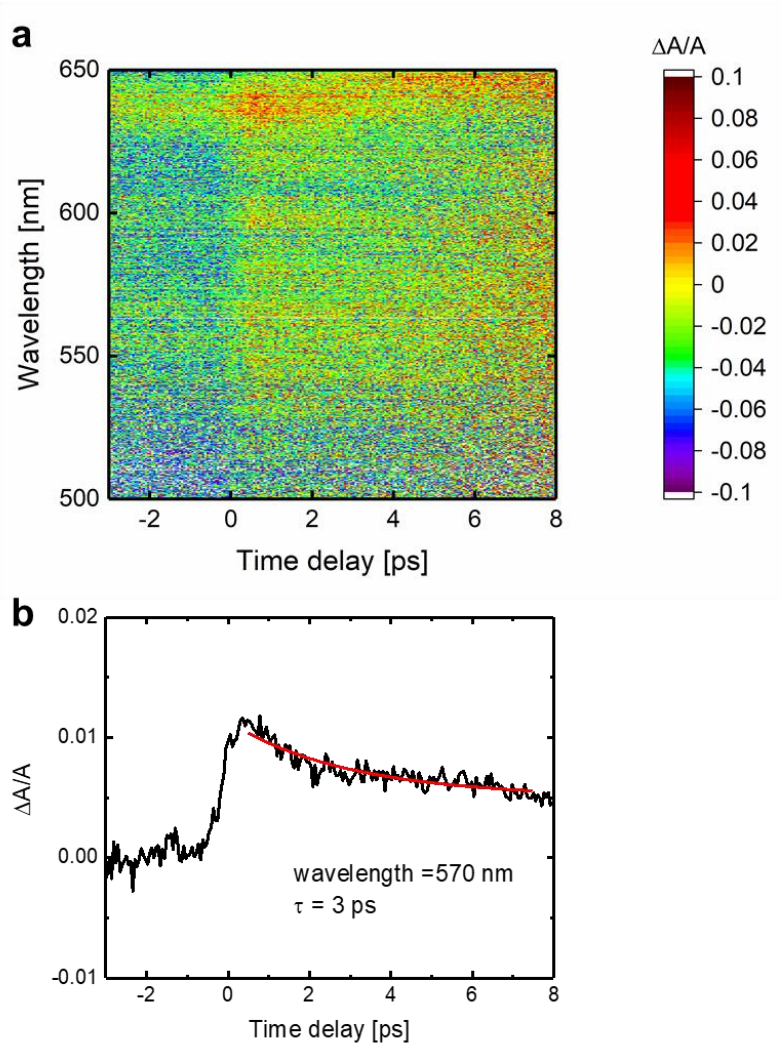


Figure S20. Multiple shot (100 shots) transient absorption spectra. (a) Two-dimensional map of repetitive transient absorption as functions of the time delay and wavelength. One hundred pump-probe experiments were repetitively performed on the same sample spot to acquire an image. The incident fluence of the UV pulse (wavelength of 266 nm and pulse duration of 120 fs) was set to 0.75 mJ/cm$^2$. (b) Transient absorption spectrum at a wavelength of 570 nm. The red line is the fit obtained using an exponential decay curve with a decay time of 3 ps and a constant offset, probably due to components with long decay times.

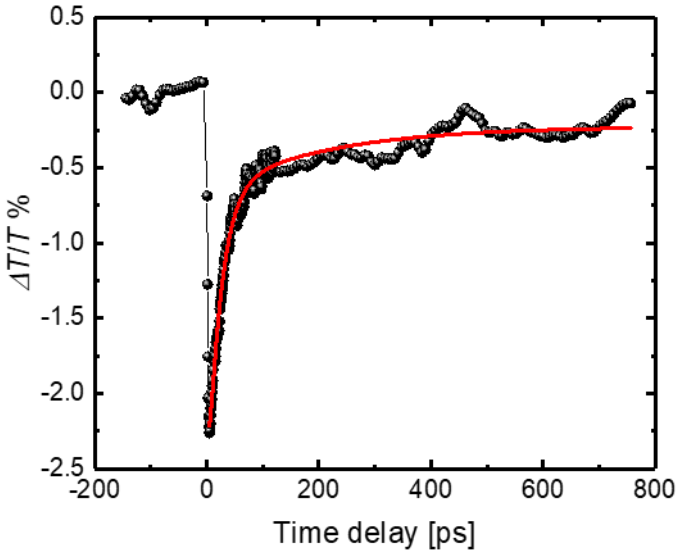


Figure S21. Transient transmission spectrum obtained from repeated measurements. Transient transmission experiments with pump and probe pulse wavelengths of 266 nm (third harmonic generation of Ti: sapphire regenerative laser) and 400 nm (second harmonic generation of Ti: sapphire regenerative laser), respectively, were performed. The incident fluence, pulse duration, and repetition of the pump UV pulses were 2 mJ/cm$^2$, ~100 fs, and 500 Hz, respectively. The pulse duration and repetition rate of the probe pulses were ~100 fs and 1 kHz, respectively. The signal of the probe light moderated at 500 Hz was detected using a GaP photodetector and a lock-in amplifier. The red line is the fit obtained using a double exponential decay curve with a long decay component of 205 ps.

## 4. TD-DFT calculations

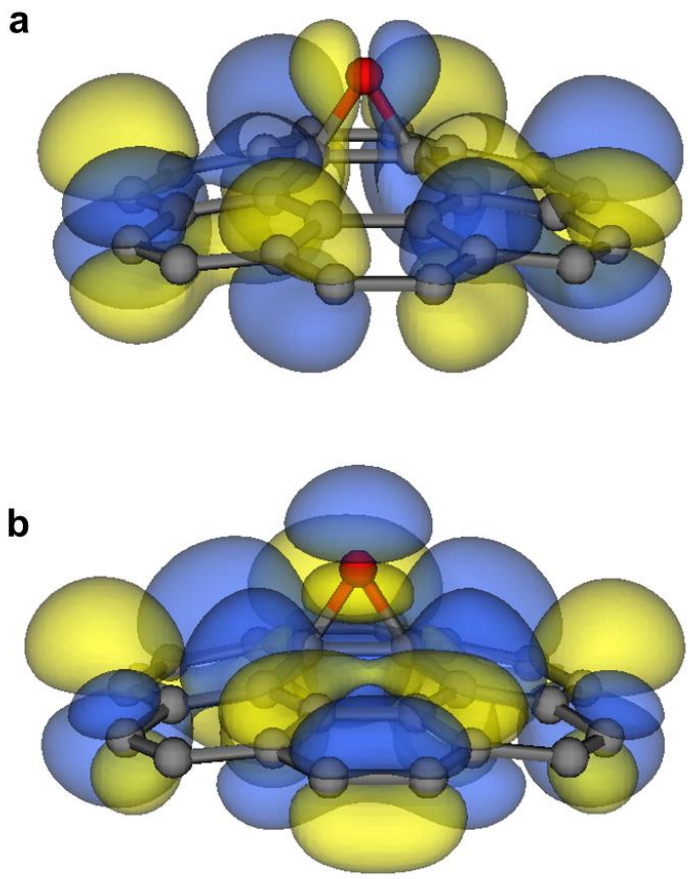


Figure S22. The spatial distributions of the wave functions of GO models (24 carbon atoms) with an epoxy oxygen in the HOMO (a) and LUMO (b). The yellow and blue colors represent isosurfaces with values of 0.015 a.u. and –0.015 a.u., respectively. The calculated C–O bond lengths of epoxy oxygen are presented in the main text (Figure 7e).

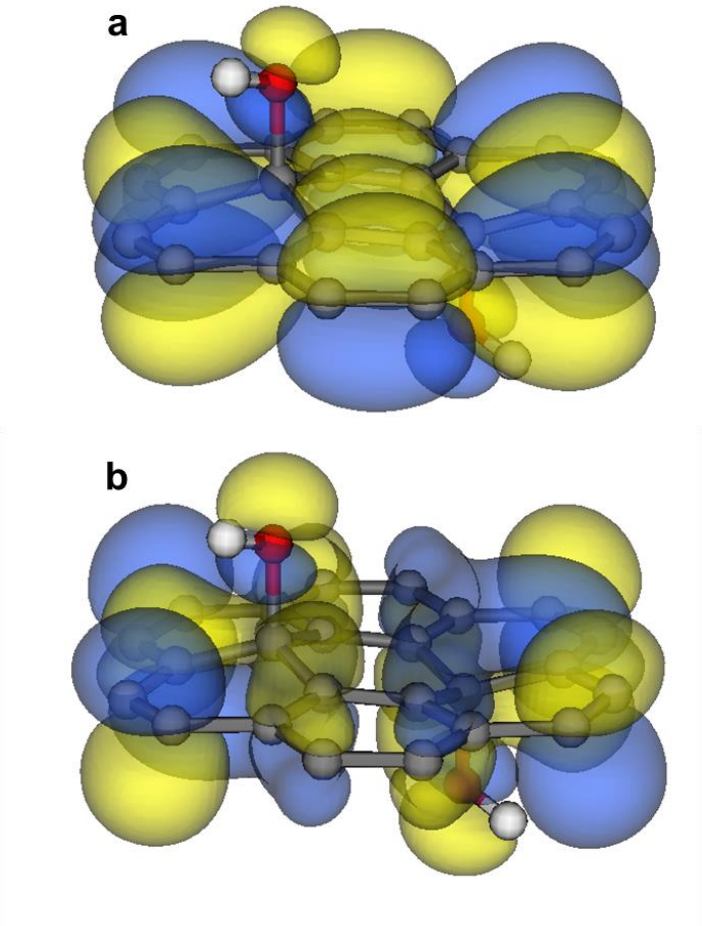


Figure S23. The spatial distributions of the wave functions of GO models (24 carbon atoms) with hydroxyl oxygens in the HOMO (a) and LUMO (b). The yellow and blue colors represent isosurfaces with values of 0.015 a.u. and –0.015 a.u., respectively. The calculated C–O bond lengths of hydroxyl oxygen are presented in the main text (Figure 7f).

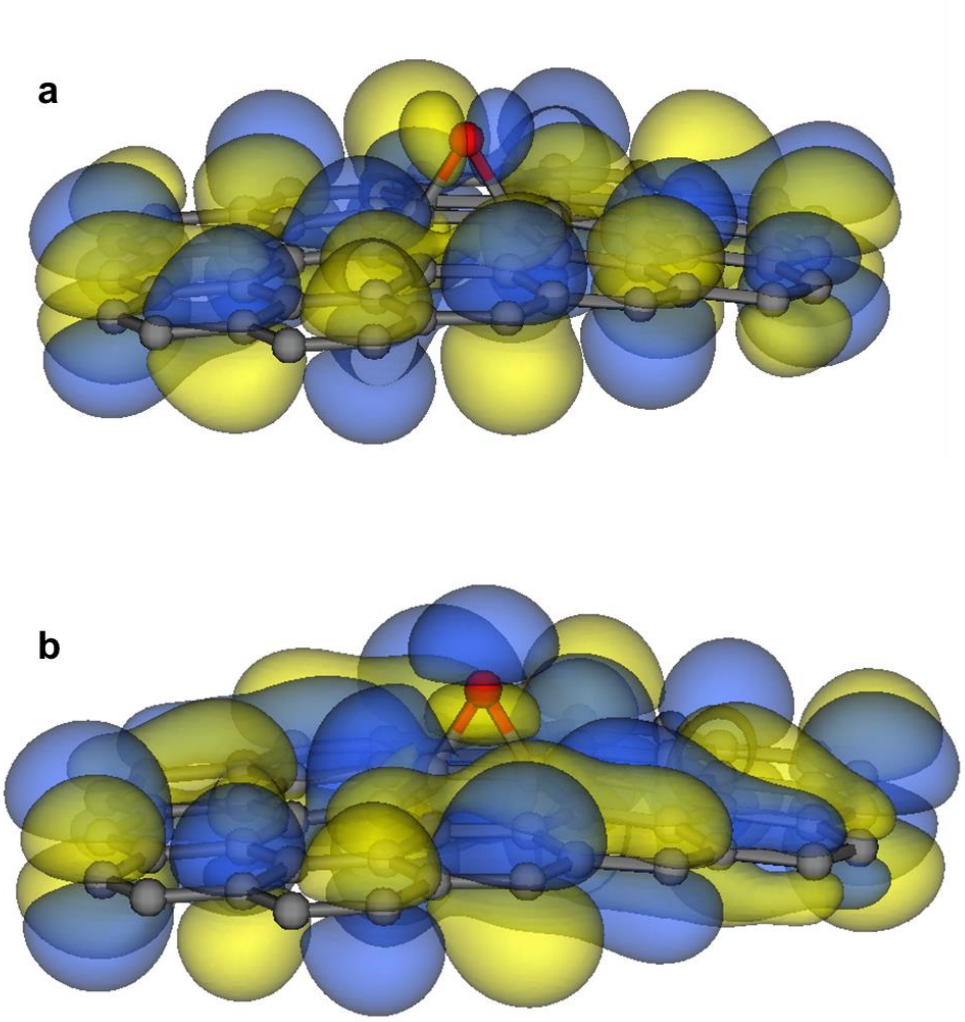


Figure S24. The spatial distributions of the wave functions of GO models (52 carbon atoms) with an epoxy oxygen in the HOMO (a) and LUMO (b). The yellow and blue colors represent isosurfaces with values of 0.015 a.u. and –0.015 a.u., respectively. The spatial distribution of the wave function essentially does not change with the size of the GO model.

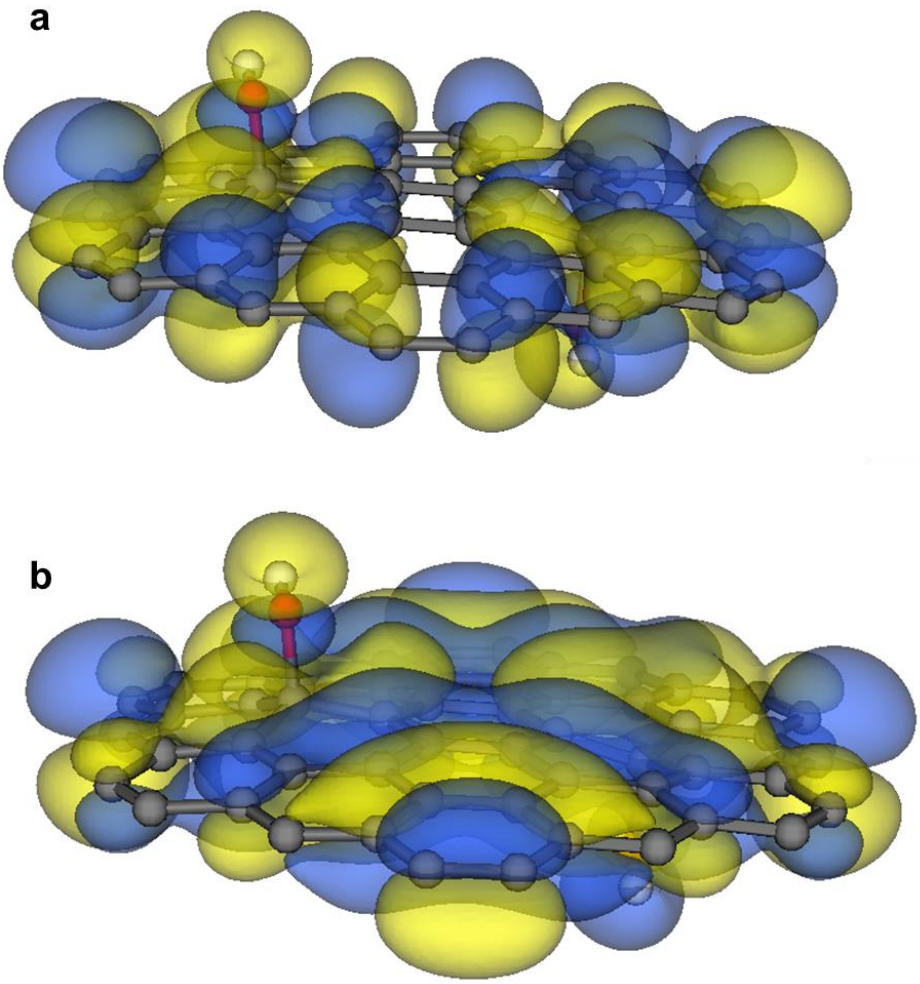


Figure S25. The spatial distributions of the wave functions of GO models (54 carbon atoms) with hydroxyl oxygens in the HOMO (a) and LUMO (b). The yellow and blue colors represent isosurfaces with values of 0.015 a.u. and –0.015 a.u., respectively. The spatial distribution of the wave function essentially does not change with the size of the GO model.

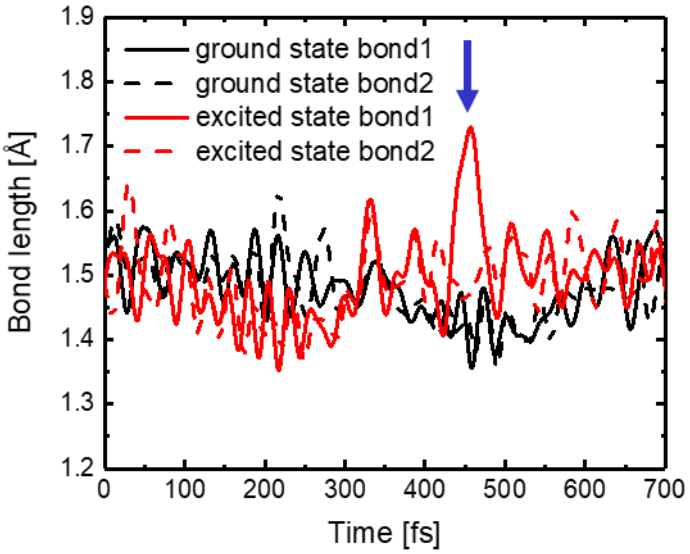


Figure S26. Calculated C–O bond lengths for an epoxy oxygen atom in the GO model shown in Figure S21 with and without excitation. The C–O bond is weakened in the excited state due to the anti-bonding character, as indicated by the blue arrow.

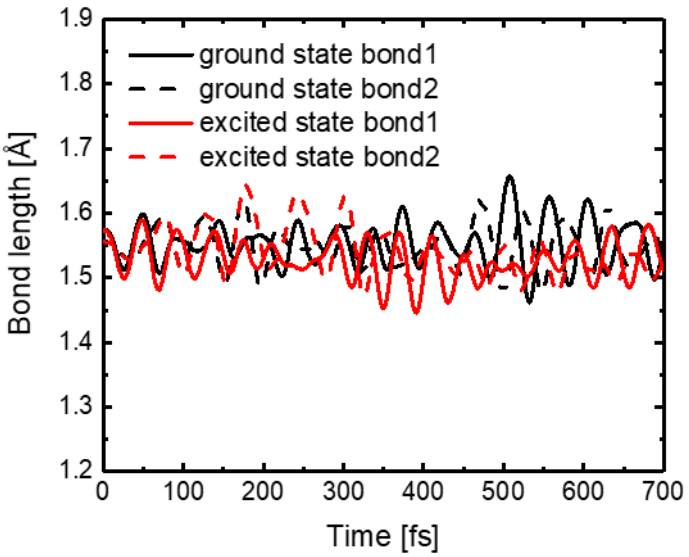


Figure S27. Calculated C–O bond lengths for hydroxyl oxygen atoms in the GO model shown in Figure S22 with and without excitation. The C–O bond is not weakened in the excited state.

## Note S1

### Numerical details

The electronic states were calculated using the projected-augmented wave (PAW)[S8,S9] method within the framework of density functional theory (DFT). We included the 2s and 2p states of C and O and the 1s state of H as the valence electrons. The generalized gradient approximation (GGA-PBE)[S10] was used to calculated the exchange-correlation energy. The electronic pseudowave functions and the pseudocharge density are expanded by plane waves with cutoff energies of 30 and 250 Ry, respectively. The energy functional is minimized with respect to the Kohn-Sham (KS) orbitals using an iterative method.[S11,S12]

We describe excited electronic states as linear combinations of electron-hole pairs within Casida's linear-response time-dependent density functional theory (LR-TDDFT),[S13–S16] using the ground-state KS orbitals as a basis set. In LR-TDDFT, electronic excitation energies are calculated from the poles of an electron-hole pair response function. This procedure amounts to solving an eigenvalue problem, with a matrix size of $N_o N_u \times N_o N_u$ when using the GGA ($N_o$ and $N_u$ are the numbers of occupied and unoccupied KS orbitals, respectively, used to represent excited states). In this study, we included HOMO-4 ~ HOMO as occupied states and LUMO~LUMO+4 as unoccupied states. Here, many-body effects are introduced by coupling matrix elements consisting of the random-phase-approximation and exchange-correlation terms.

Molecular dynamics (MD) simulations of the canonical ensemble were performed using the Nosè-Hoover thermostat technique.[S17,S18] The equations of motion were integrated numerically using an explicit reversible integrator[S19] with a time step of 20 a.u. (~ 0.48 fs). All MD simulations were performed at room temperature.

## Supporting References


S1. Nozawa, S.; Adachi, S.; Takahashi, J.; Tazaki, R.; Guérin, L.; Daimon, M.; Tomita, A.; Sato, T.; Chollet, M.; Collet, E.; Cailleau, H.; Yamamoto, S.; Tsuchiya, K.; Shioya, T.; Sasaki, H.; Mori, T.; Ichiyanagi, K.; Sawa, H.; Kawata, H.; Koshihara, S. Developing 100 Ps-Resolved X-ray Structural Analysis Capabilities on Beamline NW14A at the Photon Factory Advanced Ring. *J. Synchrotron Radiat.* **2007**, *14*, 313–319.

S2. Ichiyanagi, K.; Sato, T.; Nozawa, S.; Kim, K. H.; Lee, J. H.; Choi, J.; Tomita, A.; Ichikawa, H.; Adachi, S.; Ihee, H.; Koshihara, S. 100 Ps Time-Resolved Solution Scattering Utilizing a Wide-Bandwidth X-ray Beam from Multilayer Optics. *J. Synchrotron Radiat.* **2009**, *16*, 391–394.

S3. Gómez-Navarro, C.; Meyer, J. C.; Sundaram, R. S.; Chuvilin, A.; Kurasch, S.; Burghard, M.; Kern, K.; Kaiser, U. Atomic Structure of Reduced Graphene Oxide. *Nano Lett.* **2010**, *10*, 1144–1148.

S4. Wyckof, R. W. G. In *Crystal Structures, 2nd edition*; Interscience publishers: New York, 1963; pp. 7–83.

S5. Morioku, K.; Morimoto, N.; Takeuchi, Y.; Nishina, Y. Concurrent Formation of Carbon–Carbon Bonds and Functionalized Graphene by Oxidative Carbon-Hydrogen Coupling Reaction. *Sci. Rep.* **6**, 25824 (2016).

S6. Su, C.; Loh, K. P. Carbocatalysts: Graphene Oxide and Its Derivatives. *Acc. Chem. Res.* **2013**, *46*, 2275–2285.

S7. Takeda, J.; Oba, W.; Minami, Y.; Saiki, T.; Katayama I. Ultrafast Crystalline-to-Amorphous Phase Transition in $Ge_2Sb_2Te_5$ Chalcogenide Alloy Thin Film Using Single-Shot Imaging Spectroscopy. *Appl. Phys. Lett.* **2014**, *104*, 261903.

S8. Blöchl, P. E. Projector Augmented-Wave Method. *Phys. Rev. B* **1994**, *50*, 17953–17979.

S9. Kresse, G.; Joubert, D. From Ultrasoft Pseudopotentials to the Projector Augmented-Wave Method. *Phys. Rev. B* **1999**, *59*, 1758–1775.

S10. Perdew, J. P.; Burke, K.; Ernzerhof, M. Generalized Gradient Approximation Made Simple. *Phys. Rev. Lett.* **1996**, *77*, 3865–3868.

S11. Kresse, G.; Hafner, J. *Ab Initio* Molecular-Dynamics Simulation of the Liquid-Metal–Amorphous-Semiconductor Transition in Germanium. *Phys. Rev. B* **1994**, *49*, 14251–14269.

S12. Shimojo, F.; Kalia, R. K.; Nakano, A.; Vashishta, P. Linear-Scaling Density-Functional-Theory Calculations of Electronic Structure Based on Real-Space

Grids: Design, Analysis, and Scalability Test of Parallel Algorithms. *Comput. Phys. Commun.* **2001**, *140*, 303–314.

S13. Casida, M. E. Recent Advances in Computational Chemistry: Volume 1. In *Recent Advances in Density Functional Methods (part I)*; Chong, D. P., Ed.; World Scientific: Singapore, 1995; pp. 155–192.

S14. Hirai, H.; Sugino, O. A Time-Dependent Density-Functional Approach to Nonadiabatic Electron-Nucleus Dynamics: Formulation and Photochemical Application. *Phys. Chem. Chem. Phys.* **2009**, *11*, 4570–4578.

S15. Walter, M.; Häkkinen, H.; Lehtovaara, L.; Puska, M.; Enkovaara, J.; Rostgaard, C.; Mortensen, J. J. Time-Dependent Density-Functional Theory in the Projector Augmented-Wave Method. *J. Chem. Phys.* **2008**, *128*, 244101.

S16. Tapavicza, E.; Tavernelli, I.; Rothlisberger, U. Trajectory Surface Hopping within Linear Response Time-Dependent Density-Functional Theory. *Phys. Rev. Lett.* **2007**, *98*, 023001.

S17. Nosé, S. A Molecular Dynamics Method for Simulations in the Canonical Ensemble. *Mol. Phys.* **1984**, *52*, 255–268.

S18. Hoover, W. G. Canonical Dynamics: Equilibrium Phase-Space Distributions. *Phys. Rev. A* **1985**, *31*, 1695–1697.

S19. Tuckerman, M.; Berne, B. J.; Martyna, G. J. Reversible Multiple Time Scale Molecular Dynamics. *J. Chem. Phys.* **1992**, *97*, 1990–2001.